HHS Public Access

Author manuscript

Nanomedicine. Author manuscript; available in PMC 2019 April 01.

Published in final edited form as:

Nanomedicine. 2018 April ; 14(3): 789–799. doi:10.1016/j.nano.2017.12.014.

Imaging-guided photo-therapeutic nanoporphyrin synergized HSP90 inhibitor in patient-derived xenograft bladder cancer model

Qilai Long[1,2,§], **Tzu-yin Lin**[2,§], **Yee Huang**[3,4], **Xiaocen Li**[3], **Ai-hong Ma**[2], **Hongyong Zhang**[2], **Randy Carney**[3], **Susan Airhart**[5], **Kit S Lam**[3], **Chong-xian Pan**[2,6,7,*], and **Yuanpei Li**[3,*]

[1]Department of Urology, Zhongshan Hospital, Fudan University, Shanghai, China 200032

[2]Department of Internal Medicine, University of California Davis, Sacramento, CA 95817, USA

[3]Department of Biochemistry and Molecular Medicine, University of California Davis, Sacramento, CA 95817, USA

[4]Institute of Animal Husbandry and Veterinary Science, Zhejiang Academy of Agricultural Sciences

[5]The Jackson Laboratory, Bar Harbor, Maine, USA

[6]Department of Urology, University of California Davis, Sacramento, CA 95817, USA

[7]VA Northern California Health Care System, Mather, CA

Abstract

Photodynamic therapy is a promising and effective non-invasive therapeutic approach for the treatment of bladder cancers. Therapies targeting HSP90 have the advantage of tumor cell selectivity and have shown great preclinical efficacy. In this study, we evaluated a novel multifunctional nanoporphyrin platform loaded with an HSP90 inhibitor 17AAG (NP-AAG) for use as a multi-modality therapy against bladder cancer. NP-AAG was efficiently accumulated and retained at bladder cancer patient-derived xenograft (PDX) over 7 days. PDX tumors could be synergistically eradicated with a single intravenous injection of NP-AAG followed by multiple light treatments within 7 days. NP-AAG mediated treatment could not only specifically deliver 17AAG and produce heat and reactive oxygen species, but also more effectively inhibit essential bladder cancer essential signaling molecules like Akt, Src, and Erk, as well as HIF-1α induced by photo-therapy. This multifunctional nanoplatform has high clinical relevance and could dramatically improve management for bladder cancers with minimal toxicity.

Graphical abstract

Corresponding Authors: Yuanpei Li, Chong-xian Pan, Address: 2700 Stockton Blvd, Sacramento, CA 95817 USA, Phone: 916-473-4420, lypli@ucdavis.edu; cxpan@ucdavis.edu.

[§]These authors had equal contribution

HSP90 inhibitor, 17-AAG, loaded nanoporphyrin formed a “triple whammy” to eradicate bladder cancers via photodynamic therapy, photothermal therapy, and targeted therapy. Prolonged tumor accumulation of HSPP90 inhibitors not only efficiently prevented the photo-therapy induced HIF1α, but also downregulated several essential signaling molecules, such as Akt, Src, and Erk in bladder cancer resulting in superior anti-cancer effect in patient derived xenograft model.

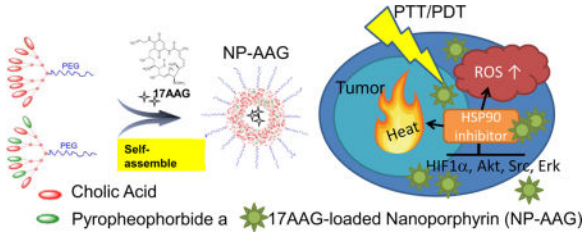

Keywords

photodynamic therapy; photothermal therapy; HSP90 inhibitor; bladder cancer; nanoparticle

Introduction

Urothelial carcinomas originate from the epithelial cells of the inner lining of the urinary track. It is the second most common malignancy affecting the urinary system. In 2016, about 76,960 new patients were diagnosed with bladder cancer, whereas 16,390 died from this disease(1). Frequent recurrence and disease progression are the characteristic features of urothelial carcinomas, as approximately 60% of patients with non-myoinvasive bladder cancer experience recurrence, and 25% progress to advanced stages in two years (2–4). Due to its high recurrence rate, the cost per patient for bladder cancer is the highest among all malignancies(5). The high recurrence rates are due to residual tumor missed during resection or undetectable microscopic lesions under white light endoscope (6–8). Either intravesical injection of bacillus Calmette–Guérin (BCG) or administration of chemotherapeutic drugs have been used after transurethral resection to prevent bladder cancer recurrence. However, the response rate is only around 20%-40% (9, 10). For myoinvasive bladder cancer, approximately half of all patients develop distant cancer recurrence after cystectomy, and ultimately succumb to the disease (11). Therefore, a major unmet clinical need is for more effective therapeutic options to minimize the recurrence rate and surveillance frequency.

Photodynamic therapy (PDT) is a promising and efficient non-invasive therapeutic method approved for the treatment of several types of cancers, including esophageal and lung cancers. PDT-based cancer treatment encompasses administration of a photosensitizer followed by illumination at the tumor site with light, a process which significantly reduces side effects and improves target specificity (12). Undergoing the type 2 reaction, PDT results in the production of singlet oxygen species and therefore subsequent tumor cell apoptosis, vascular structure damage, and inflammatory response (13). Using a PDT approach, clinical trials revealed a complete response rate of 80% and 50% for carcinoma in situ and papillary tumors at 3 months, respectively (14). Although promising, and with many improvements compared to conventional therapies, the clinical applications of PDT are still hampered by

poor water solubility of the photosensitizers used to elicit the PDT effect, moderate tissue specificity, and some side effects, including phototoxicity and hypoxic tumor microenvironment (15–17). In contrast, photothermal therapy (PTT) is a viable alternative that addresses many of these pitfalls. PTT-induced local hyperthermia causes cancerous cell apoptosis and necrosis. PTT had been shown to enhance anti-cancer efficacy along with either PDT or chemotherapy (18, 19). Though still in its developmental stage for the treatment of bladder cancer, several inorganic nanomaterials and single-walled carbon nanocarrier were developed for potential PTT on urothelial carcinoma cell lines (20, 21). To further advance this technology, a newer generation of tumor targeting nano-delivery system and a combination with other molecularly targeted molecules to mitigate PDT related resistance would be desirable.

Heat shock protein 90 (HSP90) is an important chaperone that regulates the folding, maturation, conformation, and stability of a number of proteins involved in cell proliferation, differentiation, survival and various signal pathways(22). Bladder cancers are genetically complex and carry multiple mutations, thus greatly rely on HSP90 chaperone for their oncogenesis (23). Cells upregulate HSP90 expressions in response to PDT, resulting in a potential mechanism for resistance (24, 25). In addition, PDT was found to induce expression of various pro-survival and angiogenic signaling molecules, such as Akt, HIF-1α, and VEGF in tumor tissue which further attenuate the efficacy of PDT (26, 27). Ferrario et al also showed the promising synergistic anti-cancer effects between PDT and HSP90 inhibitors in breast cancers. (26, 28) Furthermore, the up-regulation of HSP90 in response to hyperthermia also contributes to thermoresistance, while combination thermal therapy with an HSP90 inhibitor 17-allylamino-17-demethoxygeldanamycin (17AAG) significantly promoted tumor cell apoptosis (29, 30). Collectively, inhibition of HSP90 not only downregulates major oncogenic drivers like Akt, Erk, and Src, resulting in reduced cell proliferation and viability (31), but also potentially overcomes HSP90 mediated resistance following PDT and thermal therapy(26).

Recently, our group has developed a novel all-in-one nanoporphyrin (NP) platform that integrates broad imaging and therapeutic functions, including near infrared fluorescence imaging (NIRFI), PDT, PTT, and targeted drug delivery (32). NP particles can efficiently encapsulate poorly water-soluble 17AAG to form NP-AAG, which display anti-cancer activities against prostate cancer (33). In this project, we studied the potential synergistic effects of NP-AAG against bladder cancer cell lines, and confirmed its superior efficacy in a patient-derived xenograft (PDX) bladder cancer model with single injection followed by imaging-guided laser treatments. These effects were observed with targeted 17AAG delivery to the tumor sites alongside better inhibitions of HIF-1α, Akt, Erk, and Src.

Methods

Animal models, cell lines and other materials

The PDX (BL0382, JAX Model # TM00020) model was kindly provided by The Jackson Laboratory (Sacramento, CA). It was developed from an 88-year-old female patient with cT2NxMx high-grade urothelial carcinoma with lymphovascular invasion. Human bladder cancer cell lines (T24, J82, 5637) were obtained from the American Type Culture Collection

(Manassas, VA), and were cultured with the recommended medium supplemented with 10 % fetal bovine serum (Gibco, Grand Island, NY) and 1% penicillin– streptomycin (Gibco) at 37°C with 5% CO2.

Synthesis and characterization of NP-AAG

Porphyrin-based telodendrimer and telodendrimer $PEG^{5K}CA_8$ were synthesized as previously described(32, 33). 17AAG at 1 mg/mL was loaded in the mixture of 10 mg/mL porphyrin-based telodendrimer and 10 mg/mL $PEG^{5K}CA_8$ to form the nanoporphyrin-loaded 17AAG (NP-AAG) used for *in vitro* studies. 17AAG at 4 mg/mL was loaded in the mixture of 2.5 mg/mL porphyrin-based telodendrimer and 17.5 mg/mL $PEG^{5K}CA_8$ for animal studies. Empty NPs with identical ratios of telodendrimers were prepared as control groups. The amount of the NP was comparable with our previous known effective concentrations (32, 33). The size and morphology of NP-AAG were characterized by dynamic light scattering (DLS) and transmission electron microscopy (TEM), respectively.

Cellular uptake of NP-AAG

T24 and 5637 cells were cultured on 8 well chamber slides overnight. Samples were treated with NP-AAG (NPs: 10 μg/mL, 17AAG: 1 μg/mL) for 4 hr, and images were acquired using a Zeiss confocal microscope (LSM 800, Zeiss, Germany) without washing or fixation. Nuclei were counterstained with Hoechst 33342 (Invitrogen).

In vivo mouse optical imaging and cellular uptake

BL0382 PDX models were established in NOD.Cg-*Prkdc*^{scid} *Il2rg*^{tm1Wjl}/SzJ (NSG) mice (The Jackson Laboratory, Stock #005557) as previously described (34), and NP-AAG was intravenously injected (NPs: 25 mg/kg, 17AAG: 40 mg/kg). Two or seven days later, NIRFI was acquired by Kodak imaging system IS2000MM. After imaging, mice were sacrificed and tumor and major organs were harvested for *ex vivo* imaging. For *in vivo* tumor cell uptake, another set of mice bearing subcutaneous BL0382 PDX were intravenously injected with NP-AAG. Mice were sacrificed 48 hr later and tumor tissues were digested into single cell suspensions. Cells were analysed by flow cytometry (Beckman Coulter, Miami, FL).

Cell viability and apoptosis assays

For cell viability assay, bladder cancer cell lines T24, J82 and 5637 were each seeded at 5000 cells/100 μL/well overnight and then treated with NP-AAG, NP alone and free 17AAG at the indicated concentrations for 24 hr. The drugs were then removed and replaced with fresh medium followed by NIR light treatment for 2 min (Omnilux New-U LED panel, 635nm, 13 mW) according to prior studies (32, 35). Cell viability decrease was measured after another 48 hr using MTS assay (Promega, Maddison, WI) according to the manufacture's protocol. For the cell apoptosis assay, T24 and J82 cells were treated with PBS, NP, 17AAG, or NP-AAG for 24 hr and then washed with PBS. Cells were then treated with NIR light for 2 min. After 24 hr, cells were harvested and stained with annexin-V-FITC and propidium iodide (PI) in the binding buffers for 15 min. Samples were analyzed with flow cytometry.

In vitro and *in vivo* reactive oxygen species (ROS) production

To monitor the ROS production, T24 cells were treated with 0.5 mg/mL of NP-AAG for 24 hr followed by 30 min loading with 2′, 7′- dichlorofluorescin-diacetate (DCF) (Sigma) as an indicator in 6-well plate. Cells were washed three times with PBS and replaced with fresh medium. A portion of the well was illuminated with NIR light, ROS production were analyzed by flow cytometry. For *in vivo* ROS production, tumor samples were incubated with DCF for 30 min, then after 2 minute NIR light exposure, ROS production was acquired under fluorescence microscope (Olympus) using the Metamorph program.

Western Blot analysis

Western Blot was performed as previously reported(36). Tumors were lysed and the cell lysates were subject to SDS-PAGE electrophoresis. The separated proteins were then transferred onto a PVDF membrane(Millipore). Membranes were blocked with 3% non-fat milk and incubated with primary antibodies (all purchased from Cell signaling) overnight at 4°C. The HRP conjugated secondary antibodies were incubated with the membrane after 3 times of TBST wash. ECL Plus Western Blotting Detection Reagent (SuperSignal West Pico, Thermo Scientific, Rockford, IL) were used to develop signals on the membranes.

Animal studies for therapeutic efficacy and toxicity

All animal studies were approved by the University of California Davis Institutional Animal Care and Use Committee (IACUC # 17794) and the procedures were in accordance with institutional guidelines. When tumors achieved 200–500 mm^3, mice were assigned to four groups (n = 7 mice per group), including PBS, 17AAG (40 mg/kg), NP (25 mg/kg NP), and NP-17AAG (40mg/kg 17AAG, 25mg/kg NP). Tumors of all groups were illuminated with 0.4 W laser light (680nm, Shanghai Xilong Optoelectronics Technology Co, Ltd, China) for 3 min on the second, fourth and seventh day post single injection on the day one. Tumor surface temperatures were recorded with a NIR thermal camera (FLIR, Santa Barbara, CA). Animals were monitored every day and body weight and tumor size were measured twice a week. On the third day after the last light treatment, blood samples were obtained for CBC and biochemistry analysis.

Statistics

Data are presented as mean ± standard deviation (SD). Group comparisons were carried out using one-way analysis of variance or Student's *t* test. Survival analysis was performed using the Kaplan-Meier method. Combination index (CI) values were calculated by CompuSyn (Compusyn Inc, Paramus, NJ, USA). *P* value less than 0.05 was considered statistically significant difference.

Results

Preparation and Characterization of NP-AAG

The loading capacity of 17AAG was at least 4 mg/mL for NP with >85%% loading efficiency. NP-AAG was sphere in shape (Figure 1A) and around 20+/− 7 nm in diameter

(Figure 1B) with a narrow distribution. The poly dispersity index (PDI) of NP-AAG was 0.394 while the average zeta potential was 1.07 mV.

Efficient bladder cellular uptake of NP-AAG

To examine whether NP-AAG could be efficiently taken up by bladder cancer cells, T24 and 5637 bladder cancer cells were treated with NP-AAG for 4 hr and immediately subject to imaging analysis without wash or fixation. NP-AAG was found mainly in the cytoplasm in a diffuse pattern with multiple scattered small aggregates (Figure 2). Our previous study showed that fluorescence of NP was architecture-dependent(33). In the other words, when NP remained intact micelles, fluorescence was quenched due to $\pi - \pi$ stacking effects; when NP broke-down as single polymers, fluorescence was recovered. In the cell culture condition, there was minimal fluorescence at the background even without removing the NP-AAG because NP-AAG retained the micelle structure in the medium and thus fluorescence was quenched. The results from the present study confirmed that NP-AAG could be efficiently internalized by bladder cancer cells and disassociation of NP-AAG inside the cells led to release of fluorescence signals upon light excitation.

Selectively accumulation of NP-AAG at tumor sites

Taking advantage of the intrinsic fluorescence of NP-AAG, we monitored the *in vivo* biodistribution by NIR fluorescence imaging. The imaging was acquired at 48 hr and day 7 post intravenous injection of NP-AAG in NSG mice bearing subcutaneous PDX models (Figure 3A). Significant accumulation of NIR fluorescence signal from NP-AAG was detected at the tumor sites up to 7 days. Consistent with the *in vivo* finding, *ex vivo* imaging revealed the selective and preferable accumulation of NP-AAG at the tumor sites over other major organs, such as liver, spleen, lung, and kidney (Figure 3B). Since there was a minimal signal in the skin, our formulation may have low skin phototoxicity which is a significant clinical drawback of free photosensitizers currently in clinical use. To further investigate whether accumulated NIR signals were due to bladder cancer cell uptake, we harvested tumor xenografts at 48 hr post NP-AAG injection. The intra-tumor-cell uptake of NP-AAG was confirmed when compared to PBS group (Figure 3C). Collectively, NP-AAG preferably accumulated at the tumor sites presumably via the enhanced permeability and retention (EPR) effect with a long retention time (at least 7 days) and were internalized by the bladder cancer cells after intravenous administration.

NP-AAG mediated synergistic anti-tumor effect *in vitro*

To further test the anti-tumor effect of 17AAG and NP mediated PDT, we treated 3 bladder cell lines (T24, J82, 5637) with an increasing concentration of 17AAG, NP, and NP-AAG, with or without light treatments. The MTS results showed that while bladder cancer cell lines had only a moderate response toward 17AAG treatment (Figure 4A), a strong synergistic effect was observed with NP-AAG as evident by the combination index less than 0.3 at higher concentrations (0.5–2 μg/ml) (Figure 4B). This study also demonstrated that 17AAG could be release from NP after cellular uptake, resulting in increased cell death.

As PDT mediates tumor cell death through apoptosis, we performed apoptosis assay on T24 and J82 cells treated with 17AAG, NP and NP-AAG plus light. The results showed that NP-

AAG mediated combination therapy caused significantly increased cell death (Annevin V +/PI+) than for either control, 17AAG, or NP groups (Figure 5A & B), which implied that NP-AAG mediated combination therapy induced more apoptosis and/or necrosis mediated cell death (both cell death mechanisms could cause increased Annevin V+/PI+ cells), resulting in more loss of cell viability (Figure 5A & B).

Imaging-guided synergistic combination therapy with NPAAG *in vivo*

Given the encouraging *in vitro* results supporting a strong synergistic effect of NP-AAG mediated light treatment, we further validated these findings with the *in vivo* efficacy studies of NP-AAG in the bladder cancer PDX animal models. NSG mice with established BL0382 PDX tumors (200–500 mm^3) were treated with PBS, 17AAG free drug (dose: 40 mg/kg), NP, NP-AAG (17AAG dose: 40mg/kg; NP dose: 25 mg/kg). A biodistribution study showed a prolonged NP-AAG accumulation and retention at the tumor sites for at least 7 days (Figure 2A), allowing imaging-guided interventions. This result suggested that there was a very long time window for light treatment even with just one single injection. Therefore, we illuminated tumors multiples times on day 2, 4, and 7 after confirming the drug accumulation with NIRF imaging. As shown in Figure 6A, 17AAG alone showed minimal anti-tumor effect, yet as it was administered as a single dose, the total dose was much lower than other reported values (37–39). NP mediated photo-therapy showed moderate anti-tumor effect compared to both PBS and 17AAG groups. More impressively, the combination therapy with NP-AAG mediated phototherapy exhibited significantly superior anti-cancer efficacy comparing to NP and 17AAG groups. There was no significant difference in body weight changes, suggesting minimal systemic toxicity in all groups (Fig 6B). Given that tumor size measurements are not always accurate, especially for photo-therapy, we terminated animals on day 22 and harvested and weighed the tumors. In agreement with our tumor growth curve results, NP and NP-AAG groups had significantly smaller tumors compared to PBS control and 17AAG treated groups (Fig 6 C).

Besides changes in body weight, potential toxicities associated with the treatment groups were further evaluated by complete blood count (CBC) and serum chemistry 3 days after the last dose of light treatment in the efficacy study. All parameters were within normal limits and no significance differences were noted between groups (Table 1 and 2), indicating no significant general toxicity.

Molecular mechanisms of NP-AAG mediated combination therapy

NP mediated cell death is due to singlet oxygen generation, resulting in massive cellular oxidation damage, heat production and subsequent thermal cellular destruction (40). Even after loading with 17AAG, NP-AAG still produced intracellular ROS production *in vitro* and *in vivo* (Fig 7 A & B), similar to NP only (32). Meanwhile, even with low dose of laser treatment, the surface temperature of bladder cancer PDXs increased by approximately 15°C in the NP and NP-AAG treated groups, compared to a 5°C increase in the PBS control group (Fig 7 C). In other words, NP-AAG exhibit potent photodynamic/photothermal effects against bladder PDX cancers in mice.

We intended to explore the mechanisms of combination therapy by NP-AAG at the molecular level *in vitro* and *in vivo*. We firstly evaluated the biomarker, HSP70 for the evidence of HSP90 inhibition. HSP70 was upregulated after 17AAG, NP, and NP-AAG treatments in T24 cells and BL0382 PDX. NP-AAG treated groups had the highest HSP70 level which could be due to more efficient HSP90 inhibition or in combination of NP induced stress response. Moreover, hypoxia induced factor 1α (HIF-1α) is known to be upregulated upon PDT as part of their resistance mechanism (Fig 8) (41). Compared to NP + L treated group, NP-AAG effectively decreased their upregulation (Fig 8). Several essential molecules in the signaling pathways for bladder cancer survival, proliferation, and migration, including Akt, Erk, and Src, were downregulated with 17AAG (31, 42). In our study, in T24 cells treated with 1 μg/mL of 17AAG or BL0382 bearing mice treated with 40 mg/kg 17AAG, Akt, Erk and Src were effectively downregulated with NP-AAG, but not 17AAG at equivalent doses even when HSP90 was inhibited as evidenced by the upregulation of HSP70. Collectively, these results suggested that NP-AAG is more efficient in inhibiting HSP90, resulting in the downregulation of its client proteins *in vitro* and *in vivo*, and superior anti-cancer efficacy.

Discussion

In this project, we took an integrated approach featuring trimodal therapy (PDT, PTT, and molecular targeting) to treat non-myoinvasive bladder cancers. Since the first application to non-myoinvasive bladder cancer in 1976 by Kelly et al, PDT has become a promising non-invasive localized treatment modality for different diseases(14). Our NP formulation not only addresses issues with poor water solubility and low tissue specificity of photosensitizers, but also confers targeted delivery of hydrophobic drugs (ie. 17AAG, HSP90 inhibitor). PDT and heat stress-induced HSP90 responses were found to be one of the major resistant mechanisms. Collectively, this is the first study to show the synergistic effect between PDT, photothermal therapy, and HSP90 inhibitor in bladder cancers. In this study, we were also the first to demonstrate the superior drug delivery efficacy and combination efficacy at the molecular level in the PDX model. Over 70% of bladder cancer patients are diagnosed at non-muscle invasive (superficial) stages (2–4). This group of patients represents an ideal population for this combination therapy as the cancer is easily accessible through the transurethral approach, relatively isolated from the rest of the human body, has high disease recurrence, and there is no FDA-approved drug after disease recurrence. In particular, we measured long-term tumor accumulation that will permit flexible treatment schedules and multiple treatments with single injection or even “out-patient” based portable whole bladder illuminator device with an optical fiber installed through urethral. Therefore, this innovation is particularly important for clinical translation for bladder cancer.

This is the first study demonstrated the synergistic effects of photo-therapy combining with 17AAG in a novel nanoporphyrin platform in a PDX bladder cancer model. PDX is a novel cancer research platform, developed from uncultured clinical cancer specimens. PDXs retain the principal histological and genetic characteristics of their donor tumors and remain stable across several passages. These models are valuable for preclinical drug testing, co-clinical trials, and personalized drug selection; it has been shown that PDXs have great concordance

of response with donor patient cancers (43, 44). Therefore, our study could provide valuable preclinical data for the treatment of bladder cancer, and can be more applicable to clinic.

Synergistic effects of NP-AAG could be due to better HSP90 inhibition, prolonged drug accumulation at tumor sites, suppression of photo-therapy induced pro-survival/angiogenesis molecules and essential oncogenic molecules. Compared to free 17AAG, NP-AAG was more effective in HSP90 inhibition evidenced by higher HSP70 expression (a biomarker for HSP90 inhibition), and more effective in the inhibition of client proteins. Specifically, at the low concentration of 1 μg/mL, 17AAG free drug had minimal effects on Akt, Erk, and Src, while NP-AAG elicited strong downregulation for these client proteins. Similar results were seen in the PDX model (Fig 8). Our results demonstrated that NP-AAG was more effective in inhibition of HSP90 client proteins, HIF1α, Akt, Erk and Src, and also upregulation of HSP70, presumably contributed by increased amounts of delivered drug coupled with increased retention at the PDXs compared to free 17AAG. There were no significant molecular changes in the free 17AAG treated groups (Fig 8). This is likely because the single dose of 40 mg/kg 17AAG may simply not have enough drug concentration accumulated at tumor sites for the target modifications. Alternatively, molecular changes were more transient and usually seen only within the couple of hours post free 17AAG treatment. Thus, at 28 hr post initial injections, the signaling molecules would have possibly returned to their baseline levels. Additionally, HSP90 upregulation upon thermal therapy is reported to be associated with thermal resistance (29). It was reported that 17AAG could enhance cell apoptosis induced by thermal therapy with gold-nanoparticles, while HSP90 inhibitor-conjugated nanoparticles combined hyperthermia with inhibition of HSP90, and synergistically induced tumor cell death (45, 46). Collectively, the superior anti-bladder cancer effects of NP-AAG were contributed by the overcome of HSP90 induced resistance together with both PDT and thermal therapy.

Inhibition of Akt, Erk, and Src by NP-AAG induced bladder cancer cell death *in vitro* and *in vivo*. The expression of phosphorylated Akt was found to be associated with tumor progression and mortality in bladder cancer patients (47, 48). Since activation of Akt plays an important role in bladder cancer growth and survival, Akt becomes an attractive and effective target for treatment. Similarly, p-Erk predicts poor prognosis of bladder cancers(49), while inhibition of p-Erk with multi-kinase inhibitors, such as sorafenib, gefitinib, and metformin, results in decreased proliferation and increased apoptosis in urothelial cell lines(50, 51). Additionally, the role of Src in bladder cancers is associated with epithelial-mesenchymal transition, cell invasion, survival, and movement (52, 53). Inhibition of Src phosphorylation could induce bladder cancer cell apoptosis via the focal adhesion kinase (FAK)/PI3K/Akt pathway, and inhibit bladder cancer cell invasion and migration (52, 54). Since these three pathways are essential for tumorigenesis, NP-AAG could more effectively and simultaneously disrupt these essential signaling pathways and achieve a better anti-cancer efficacy.

Compared to free drug, NP-AAG has excellent water solubility, specific tumor targeting abilities, and extended retention, all contributing to a prolonged drug release and therapeutic window. In our study, we showed that NP-AAG could accumulate at the tumor sites for at least 7 days (Fig 3A). Therefore, with a single dose of NP-AAG, we were able to perform

light treatment 3 times with lower intensities of light (0.4W). Since PDT could promptly further induce tumor hypoxia which then limits PDT effectiveness(55), fractional light treatments (multiple light treatments with internals of dark period) may allow tumor tissue to be reoxygenated and thus achieve the best treatment results.

Based on this new development, nanotechnology enhanced photo-therapy combined with molecular therapy has a promising prospect in bladder cancer treatment. Given the strong synergistic antitumor effect, it has high potential to be translated into clinic to eradicate primary cancer, decrease cancer recurrence, and prevent disease progression into invasive stages.

Acknowledgments

Drs. Li, Pan, Lam, Lin are the inventors for nanoporphyrin (US76916-856975/212300), and may have interests for further commercialization.

This work was financially supported by the NIH/NCI (PI: Li, R01CA199668), NIH/NICHD (PI: Li, R01HD086195), DoD PRMRP Award (PI: Lam, PR121626), Cancer Center Support Grant (PI: deVere White, P30 CA093373) and ACS IRG (PI: Lin). Also, this work was supported in part by VA BLR&D Merit grant (Grant #: 1I01BX001784, PI: Pan) from the United States (U.S.) Department of Veterans Affairs Biomedical Laboratory Research and Development Program. The contents do not represent the views of the U.S. Department of Veterans Affairs or the United States Government.

Abbreviations

17AAG	17-allylamino-17-demethoxygeldanamycin
BCG	bacillus Calmette-Guerin
DCF	2′, 7′- dichlorofluorescin-diacetate
DLS	Dynamic light scattering
CI	Combination index
CBC	Complete blood count
Fa	Fraction affected
HIF-1α	Hypoxia induced factor 1α
HSP	Heat shock protein
NP-AAG	17AAG loaded-Nanoporphyrin
PDX	Patient-derived xenograft
PDT	photodynamic therapy
PTT	photothermal therapy
PI	Propidium iodide
ROS	Reactive oxygen species

PDI	Poly dispersity index
PEG	Polyethylene Glycol
NIRF	Near infrared fluorescence
NSG	NOD.Cg-Prkdc^{scid}/IL2rgtm1Wjl/SzJ
TEM	Transmission electron microscopy

References

1. Smith RA, Andrews K, Brooks D, DeSantis CE, Fedewa SA, Lortet-Tieulent J, et al. Cancer screening in the United States, 2016: A review of current American Cancer Society guidelines and current issues in cancer screening. CA: a cancer journal for clinicians. 2016; 66(2):96–114. [PubMed: 26797525]
2. Herr HW, Schwalb DM, Zhang ZF, Sogani PC, Fair WR, Whitmore WF Jr, et al. Intravesical bacillus Calmette-Guerin therapy prevents tumor progression and death from superficial bladder cancer: ten-year follow-up of a prospective randomized trial. Journal of clinical oncology : official journal of the American Society of Clinical Oncology. 1995; 13(6):1404–8. [PubMed: 7751885]
3. Herr HW, Badalament RA, Amato DA, Laudone VP, Fair WR, Whitmore WF Jr. Superficial bladder cancer treated with bacillus Calmette-Guerin: a multivariate analysis of factors affecting tumor progression. The Journal of urology. 1989; 141(1):22–9. [PubMed: 2908949]
4. Cookson MS, Herr HW, Zhang ZF, Soloway S, Sogani PC, Fair WR. The treated natural history of high risk superficial bladder cancer: 15-year outcome. The Journal of urology. 1997; 158(1):62–7. [PubMed: 9186324]
5. Botteman MF, Pashos CL, Redaelli A, Laskin B, Hauser R. The health economics of bladder cancer: a comprehensive review of the published literature. PharmacoEconomics. 2003; 21(18):1315–30. [PubMed: 14750899]
6. Fadl-Elmula I, Gorunova L, Mandahl N, Elfving P, Lundgren R, Mitelman F, et al. Cytogenetic monoclonality in multifocal uroepithelial carcinomas: evidence of intraluminal tumour seeding. British journal of cancer. 1999; 81(1):6–12. [PubMed: 10487605]
7. Sidransky D, Frost P, Von Eschenbach A, Oyasu R, Preisinger AC, Vogelstein B. Clonal origin bladder cancer. The New England journal of medicine. 1992; 326(11):737–40. [PubMed: 1445507]
8. Hafner C, Knuechel R, Stoehr R, Hartmann A. Clonality of multifocal urothelial carcinomas: 10 years of molecular genetic studies. International journal of cancer. 2002; 101(1):1–6. [PubMed: 12209580]
9. Steinberg G, Bahnson R, Brosman S, Middleton R, Wajsman Z, Wehle M. Efficacy and safety of valrubicin for the treatment of Bacillus Calmette-Guerin refractory carcinoma in situ of the bladder. The Valrubicin Study Group. The Journal of urology. 2000; 163(3):761–7. [PubMed: 10687972]
10. von der Maase H, Hansen SW, Roberts JT, Dogliotti L, Oliver T, Moore MJ, et al. Gemcitabine and cisplatin versus methotrexate, vinblastine, doxorubicin, and cisplatin in advanced or metastatic bladder cancer: results of a large, randomized, multinational, multicenter, phase III study. Journal of clinical oncology : official journal of the American Society of Clinical Oncology. 2000; 18(17): 3068–77. [PubMed: 11001674]
11. Funt SA, Rosenberg JE. Systemic, perioperative management of muscle-invasive bladder cancer and future horizons. Nature reviews Clinical oncology. 2016
12. Wachowska M, Muchowicz A, Demkow U. Immunological aspects of antitumor photodynamic therapy outcome. Central-European journal of immunology. 2015; 40(4):481–5. [PubMed: 26862314]
13. Benov L. Photodynamic therapy: current status and future directions. Medical principles and practice : international journal of the Kuwait University, Health Science Centre. 2015; 24(Suppl 1):14–28.

14. Bozzini G, Colin P, Betrouni N, Nevoux P, Ouzzane A, Puech P, et al. Photodynamic therapy in urology: what can we do now and where are we heading? Photodiagnosis and photodynamic therapy. 2012; 9(3):261–73. [PubMed: 22959806]
15. Bechet D, Couleaud P, Frochot C, Viriot ML, Guillemin F, Barberi-Heyob M. Nanoparticles as vehicles for delivery of photodynamic therapy agents. Trends in biotechnology. 2008; 26(11):612–21. [PubMed: 18804298]
16. Overholt BF, Panjehpour M, Haydek JM. Photodynamic therapy for Barrett's esophagus: follow-up in 100 patients. Gastrointestinal endoscopy. 1999; 49(1):1–7. [PubMed: 9869715]
17. Litle VR, Luketich JD, Christie NA, Buenaventura PO, Alvelo-Rivera M, McCaughan JS, et al. Photodynamic therapy as palliation for esophageal cancer: experience in 215 patients. The Annals of thoracic surgery. 2003; 76(5):1687–92. discussion 92–3. [PubMed: 14602313]
18. Liu T, Wang C, Gu X, Gong H, Cheng L, Shi X, et al. Drug delivery with PEGylated MoS2 nano-sheets for combined photothermal and chemotherapy of cancer. Advanced materials. 2014; 26(21): 3433–40. [PubMed: 24677423]
19. Yong Y, Zhou L, Gu Z, Yan L, Tian G, Zheng X, et al. WS2 nanosheet as a new photosensitizer carrier for combined photodynamic and photothermal therapy of cancer cells. Nanoscale. 2014; 6(17):10394–403. [PubMed: 25047651]
20. Cheng FY, Chen CT, Yeh CS. Comparative efficiencies of photothermal destruction of malignant cells using antibody-coated silica@Au nanoshells, hollow Au/Ag nanospheres and Au nanorods. Nanotechnology. 2009; 20(42):425104. [PubMed: 19779243]
21. Cho SK, Emoto K, Su LJ, Yang X, Flaig TW, Park W. Functionalized gold nanorods for thermal ablation treatment of bladder cancer. Journal of biomedical nanotechnology. 2014; 10(7):1267–76. [PubMed: 24804547]
22. Bagatell R, Whitesell L. Altered Hsp90 function in cancer: a unique therapeutic opportunity. Molecular cancer therapeutics. 2004; 3(8):1021–30. [PubMed: 15299085]
23. Chehab M, Caza T, Skotnicki K, Landas S, Bratslavsky G, Mollapour M, et al. Targeting Hsp90 in urothelial carcinoma. Oncotarget. 2015; 6(11):8454–73. [PubMed: 25909217]
24. Kim J, Lim H, Kim S, Cho H, Kim Y, Li X, et al. Effects of HSP27 downregulation on PDT resistance through PDT-induced autophagy in head and neck cancer cells. Oncology reports. 2016; 35(4):2237–45. [PubMed: 26820233]
25. Burke AR, Singh RN, Carroll DL, Wood JCS, D'Agostino RB, Ajayan PM, et al. The resistance of breast cancer stem cells to conventional hyperthermia and their sensitivity to nanoparticle-mediated photothermal therapy. Biomaterials. 2012; 33(10):2961–70. [PubMed: 22245557]
26. Ferrario A, Gomer CJ. Targeting the 90 kDa heat shock protein improves photodynamic therapy. Cancer letters. 2010; 289(2):188–94. [PubMed: 19733005]
27. Chen B, Pogue BW, Zhou X, O'Hara JA, Solban N, Demidenko E, et al. Effect of tumor host microenvironment on photodynamic therapy in a rat prostate tumor model. Clinical cancer research : an official journal of the American Association for Cancer Research. 2005; 11(2 Pt 1): 720–7. [PubMed: 15701861]
28. Ferrario A, Rucker N, Wong S, Luna M, Gomer CJ. Survivin, a member of the inhibitor of apoptosis family, is induced by photodynamic therapy and is a target for improving treatment response. Cancer research. 2007; 67(10):4989–95. [PubMed: 17510430]
29. Yang R, Tang QS, Miao FQ, An YL, Li MF, Han Y, et al. Inhibition of heat-shock protein 90 sensitizes liver cancer stem-like cells to magnetic hyperthermia and enhances anti-tumor effect on hepatocellular carcinoma-burdened nude mice. International journal of nanomedicine. 2015; 10:7345–58. [PubMed: 26677324]
30. Tomasovic SP, Steck PA, Heitzman D. Heat-Stress Proteins and Thermal-Resistance in Rat Mammary-Tumor Cells. Radiat Res. 1983; 95(2):399–413. [PubMed: 6611857]
31. Karkoulis PK, Stravopodis DJ, Margaritis LH, Voutsinas GE. 17-Allylamino-17-demethoxygeldanamycin induces downregulation of critical Hsp90 protein clients and results in cell cycle arrest and apoptosis of human urinary bladder cancer cells. BMC cancer. 2010; 10:481. [PubMed: 20828379]
32. Li Y, Lin TY, Luo Y, Liu Q, Xiao W, Guo W, et al. A smart and versatile theranostic nanomedicine platform based on nanoporphyrin. Nature communications. 2014; 5:4712.

33. Lin TY, Guo W, Long Q, Ma A, Liu Q, Zhang H, et al. HSP90 Inhibitor Encapsulated Photo-Theranostic Nanoparticles for Synergistic Combination Cancer Therapy. Theranostics. 2016; 6(9): 1324–35. [PubMed: 27375782]
34. Pan CX, Zhang H, Tepper CG, Lin TY, Davis RR, Keck J, et al. Development and Characterization of Bladder Cancer Patient-Derived Xenografts for Molecularly Guided Targeted Therapy. PloS one. 2015; 10(8):e0134346. [PubMed: 26270481]
35. Lin TY, Li Y, Liu Q, Chen JL, Zhang H, Lac D, et al. Novel theranostic nanoporphyrins for photodynamic diagnosis and trimodal therapy for bladder cancer. Biomaterials. 2016; 104:339–51. [PubMed: 27479049]
36. Grasso AW, Wen D, Miller CM, Rhim JS, Pretlow TG, Kung HJ. ErbB kinases and NDF signaling in human prostate cancer cells. Oncogene. 1997; 15(22):2705–16. [PubMed: 9400997]
37. Solit DB, Basso AD, Olshen AB, Scher HI, Rosen N. Inhibition of heat shock protein 90 function down-regulates Akt kinase and sensitizes tumors to Taxol. Cancer research. 2003; 63(9):2139–44. [PubMed: 12727831]
38. Yang S, Qu S, Perez-Tores M, Sawai A, Rosen N, Solit DB, et al. Association with HSP90 inhibits Cbl-mediated down-regulation of mutant epidermal growth factor receptors. Cancer research. 2006; 66(14):6990–7. [PubMed: 16849543]
39. Yoshida S, Koga F, Tatokoro M, Kawakami S, Fujii Y, Kumagai J, et al. Low-dose Hsp90 inhibitors tumor-selectively sensitize bladder cancer cells to chemoradiotherapy. Cell cycle. 2011; 10(24):4291–9. [PubMed: 22134243]
40. Bacellar IO, Tsubone TM, Pavani C, Baptista MS. Photodynamic Efficiency: From Molecular Photochemistry to Cell Death. International journal of molecular sciences. 2015; 16(9):20523–59. [PubMed: 26334268]
41. Ji Z, Yang G, Shahzidi S, Tkacz-Stachowska K, Suo Z, Nesland JM, et al. Induction of hypoxia-inducible factor-1alpha overexpression by cobalt chloride enhances cellular resistance to photodynamic therapy. Cancer letters. 2006; 244(2):182–9. [PubMed: 16427735]
42. Ma L, Sato F, Sato R, Matsubara T, Hirai K, Yamasaki M, et al. Dual targeting of heat shock proteins 90 and 70 promotes cell death and enhances the anticancer effect of chemotherapeutic agents in bladder cancer. Oncology reports. 2014; 31(6):2482–92. [PubMed: 24718854]
43. Zhang X, Claerhout S, Prat A, Dobrolecki LE, Petrovic I, Lai Q, et al. A renewable tissue resource of phenotypically stable, biologically and ethnically diverse, patient-derived human breast cancer xenograft models. Cancer research. 2013; 73(15):4885–97. [PubMed: 23737486]
44. Marangoni E, Vincent-Salomon A, Auger N, Degeorges A, Assayag F, de Cremoux P, et al. A new model of patient tumor-derived breast cancer xenografts for preclinical assays. Clinical cancer research : an official journal of the American Association for Cancer Research. 2007; 13(13): 3989–98. [PubMed: 17606733]
45. Duncan RF. Inhibition of Hsp90 function delays and impairs recovery from heat shock. The FEBS journal. 2005; 272(20):5244–56. [PubMed: 16218955]
46. Yoo D, Jeong H, Noh SH, Lee JH, Cheon J. Magnetically Triggered Dual Functional Nanoparticles for Resistance-Free Apoptotic Hyperthermia. Angew Chem Int Edit. 2013; 52(49):13047–51.
47. Sun CH, Chang YH, Pan CC. Activation of the PI3K/Akt/mTOR pathway correlates with tumour progression and reduced survival in patients with urothelial carcinoma of the urinary bladder. Histopathology. 2011; 58(7):1054–63. [PubMed: 21707707]
48. Koletsas N, Koletsa T, Choidas S, Anagnostopoulos K, Touloupidis S, Zaramboukas T, et al. Immunohistochemical Investigation of HER/AKT/mTOR Pathway and Cellular Adhesion Molecules in Urothelial Carcinomas. Pathology research international. 2017; 2017:6794150. [PubMed: 28210516]
49. Karlou M, Saetta AA, Korkolopoulou P, Levidou G, Papanastasiou P, Boltetsou E, et al. Activation of extracellular regulated kinases (ERK1/2) predicts poor prognosis in urothelial bladder carcinoma and is not associated with B-Raf gene mutations. Pathology. 2009; 41(4):327–34. [PubMed: 19404844]
50. Rose A, Grandoch M, vom Dorp F, Rubben H, Rosenkranz A, Fischer JW, et al. Stimulatory effects of the multi-kinase inhibitor sorafenib on human bladder cancer cells. British journal of pharmacology. 2010; 160(7):1690–8. [PubMed: 20649572]

51. Peng M, Huang Y, Tao T, Peng CY, Su Q, Xu W, et al. Metformin and gefitinib cooperate to inhibit bladder cancer growth via both AMPK and EGFR pathways joining at Akt and Erk. Scientific reports. 2016; 6:28611. [PubMed: 27334428]

52. Kong D, Chen F, Sima NI. Inhibition of focal adhesion kinase induces apoptosis in bladder cancer cells via Src and the phosphatidylinositol 3-kinase/Akt pathway. Experimental and therapeutic medicine. 2015; 10(5):1725–31. [PubMed: 26640543]

53. Thiery JP. Epithelial-mesenchymal transitions in tumour progression. Nature reviews Cancer. 2002; 2(6):442–54. [PubMed: 12189386]

54. Kong DB, Chen F, Sima N. Focal adhesion kinases crucially regulate TGFbeta-induced migration and invasion of bladder cancer cells via Src kinase and E-cadherin. OncoTargets and therapy. 2017; 10:1783–92. [PubMed: 28367061]

55. Henderson BW, Fingar VH. Relationship of tumor hypoxia and response to photodynamic treatment in an experimental mouse tumor. Cancer research. 1987; 47(12):3110–4. [PubMed: 3581062]

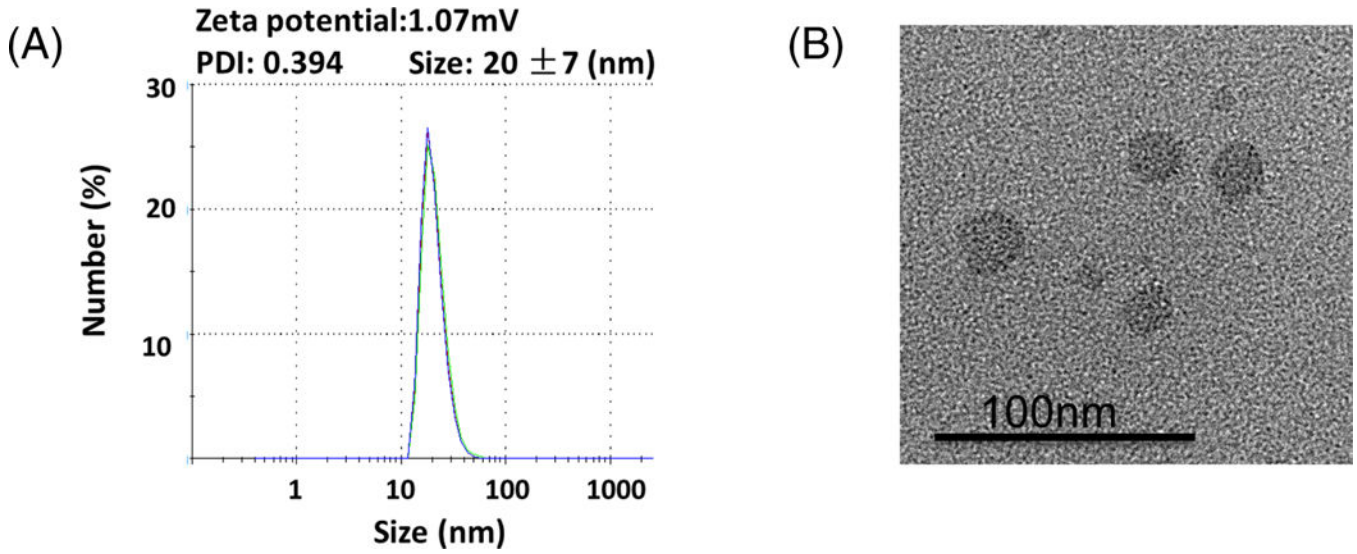

Figure 1. Characterization of NP-AAG

(A) Particle size and (B) morphology analysis for NP-AAG by dynamic light scattering (DLS) and Transmission electron microscopy (TEM), respectively. PDI: poly dispersity index

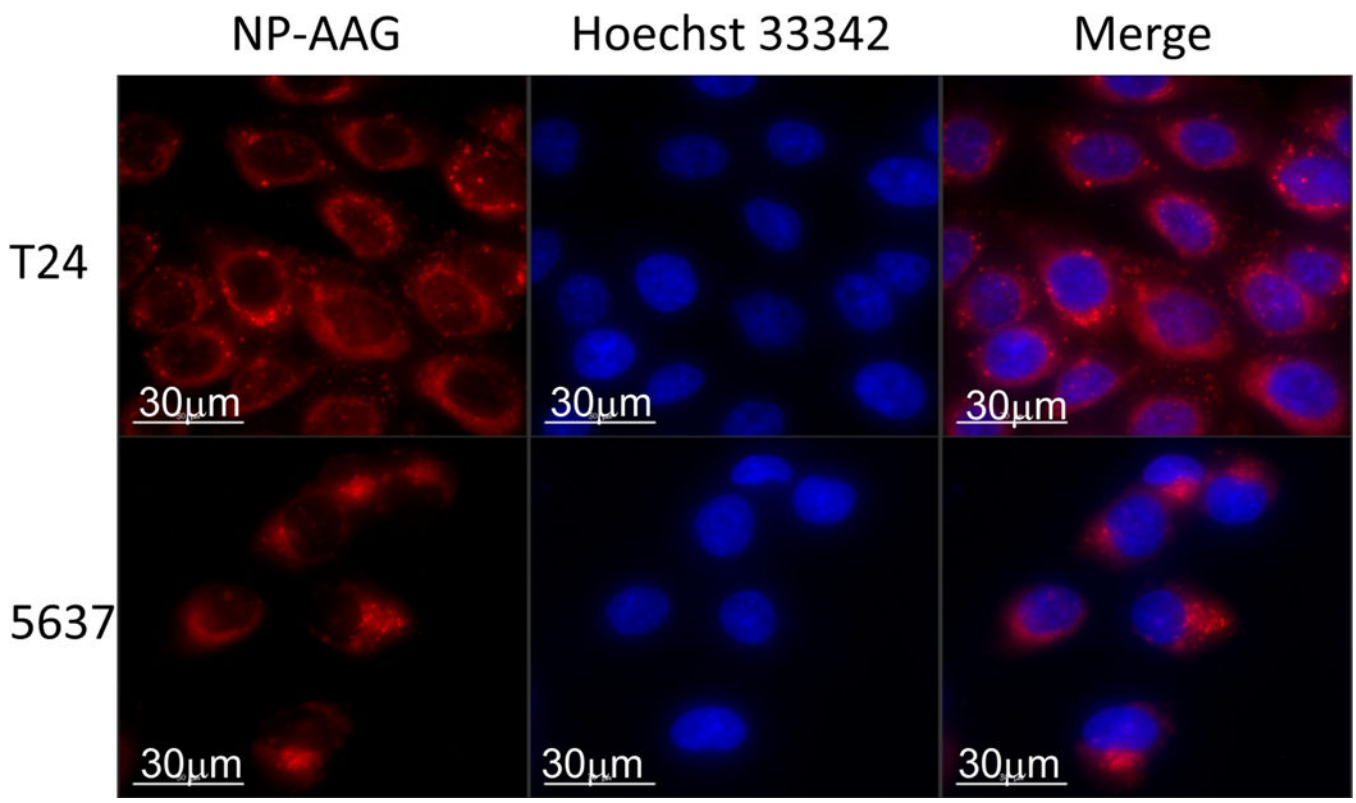

Figure 2. Cellular uptake of NP-AAG in human bladder cancer cell lines

T24 and 5637 cells were treated with 50 μg/mL of NP-AAG for 4 hr. Imaging was acquired by a DeltaVision microscopy imaging system. Nuclei were counterstained with Hoechst 33342. Bar = 30 μm.

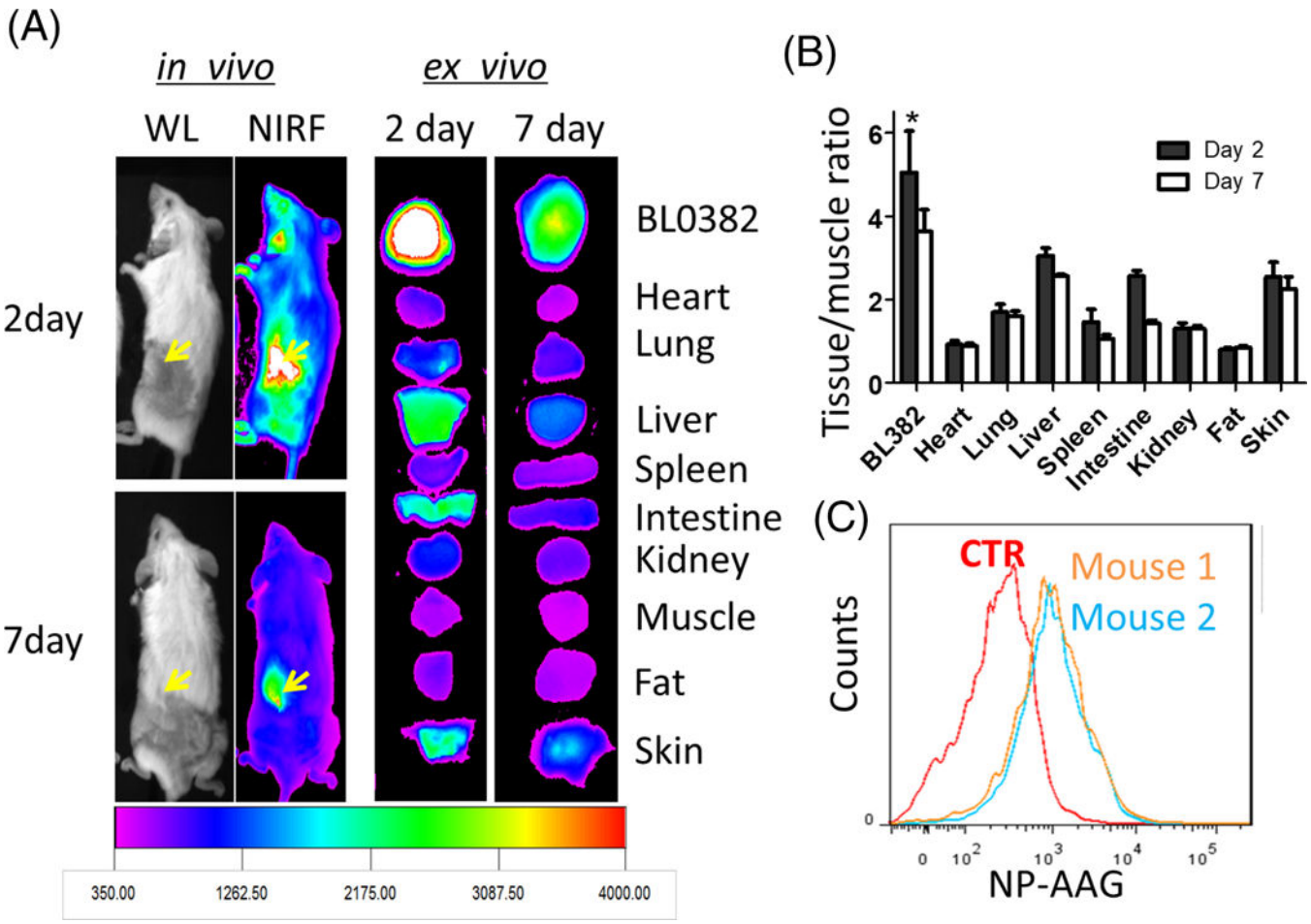

Figure 3. Specific accumulation of NP-AAG in bladder cancer PDXs

(A) *In vivo* and *ex vivo* near infrared fluorescence (NIRF) imaging of NSG mice bearing BL0382 PDXs on day 2 and 7 post a single injection of NP-AAG. Dose: 40 mg/kg 17AAG, 25 mg/kg NP. (B) Quantitative analysis of tissue or tumor NIRF signals normalized to muscle (negative control). (n=3) (C) Single bladder cancer cell analysis for the intracellular NP-AAG amount with flow cytometry. Mice were treated with PBS (Ctrl) or NP-AAG (mouse 1 and 2) (Dose: 25 mg/kg NP and 40 mg/kg 17AAG). 48 hr later, tumors were harvested and made into single cell suspensions for flow cytometry evaluation.

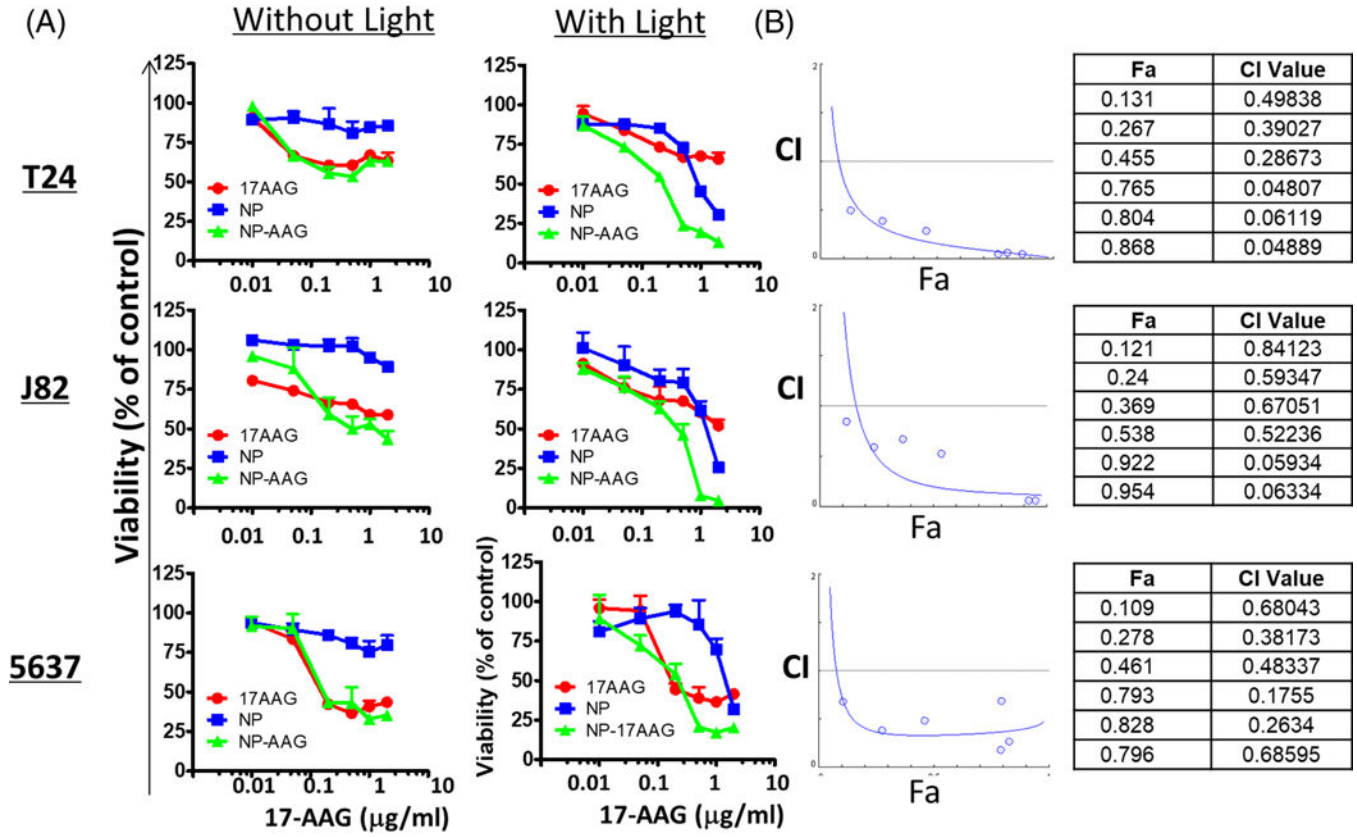

Fa	CI Value
0.131	0.49838
0.267	0.39027
0.455	0.28673
0.765	0.04807
0.804	0.06119
0.868	0.04889

Fa	CI Value
0.121	0.84123
0.24	0.59347
0.369	0.67051
0.538	0.52236
0.922	0.05934
0.954	0.06334

Fa	CI Value
0.109	0.68043
0.278	0.38173
0.461	0.48337
0.793	0.1755
0.828	0.2634
0.796	0.68595

Figure 4. Synergic anti-bladder cancer effects of NP-AAG *in vitro*

(A) Cell viability evaluation for T24, J82, and 5637 bladder cancer cell lines with 17AAG, NP, NP-AAG with or without light treatments. Cell viability was measured 48 hr post-light treatment with MTS assays. Equivalent amounts of NP were used. (B) Combination index (CI) vs. Fraction affected (Fa) plot for bladder cancer cells treated with NP, AAG, and NP-AAG followed by light treatment. CI is recognized as the standard measure of combination effect. More specifically, CI >1, =1, and <1 define antagonism, additive effect, and synergism, respectively, in drug combinations. In our study, the calculated CI for combination between photo-therapy and 17AAG was lower than 1 and thus interpreted as synergism.

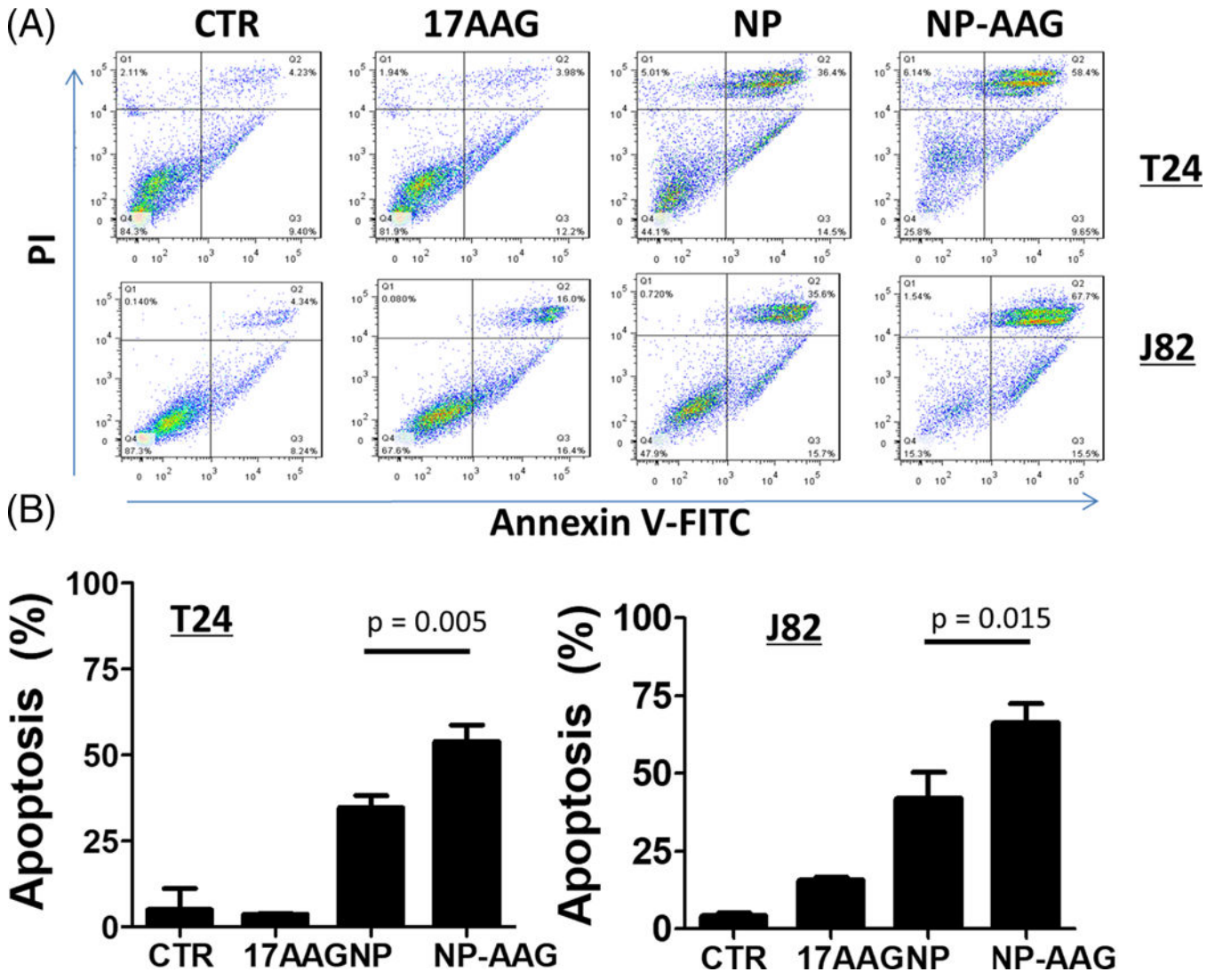

Figure 5. Cell apoptosis/necrosis analysis of NP-AAG in bladder cancer cell lines

(A) Apoptosis analysis with Annexin V-FITC/PI for T24 and J82 bladder cancer cells treated with 17AAG, NP, NP-AAG followed by light treatments. Time point: 24 hr post light treatments. (B) Quantitative analysis of percentages of late apoptosis/necrosis (Annexin V+ cells/PI+) (n=3) for T24 and J82 cells treated with 17AAG, NP, NP-AAG followed by light treatments.

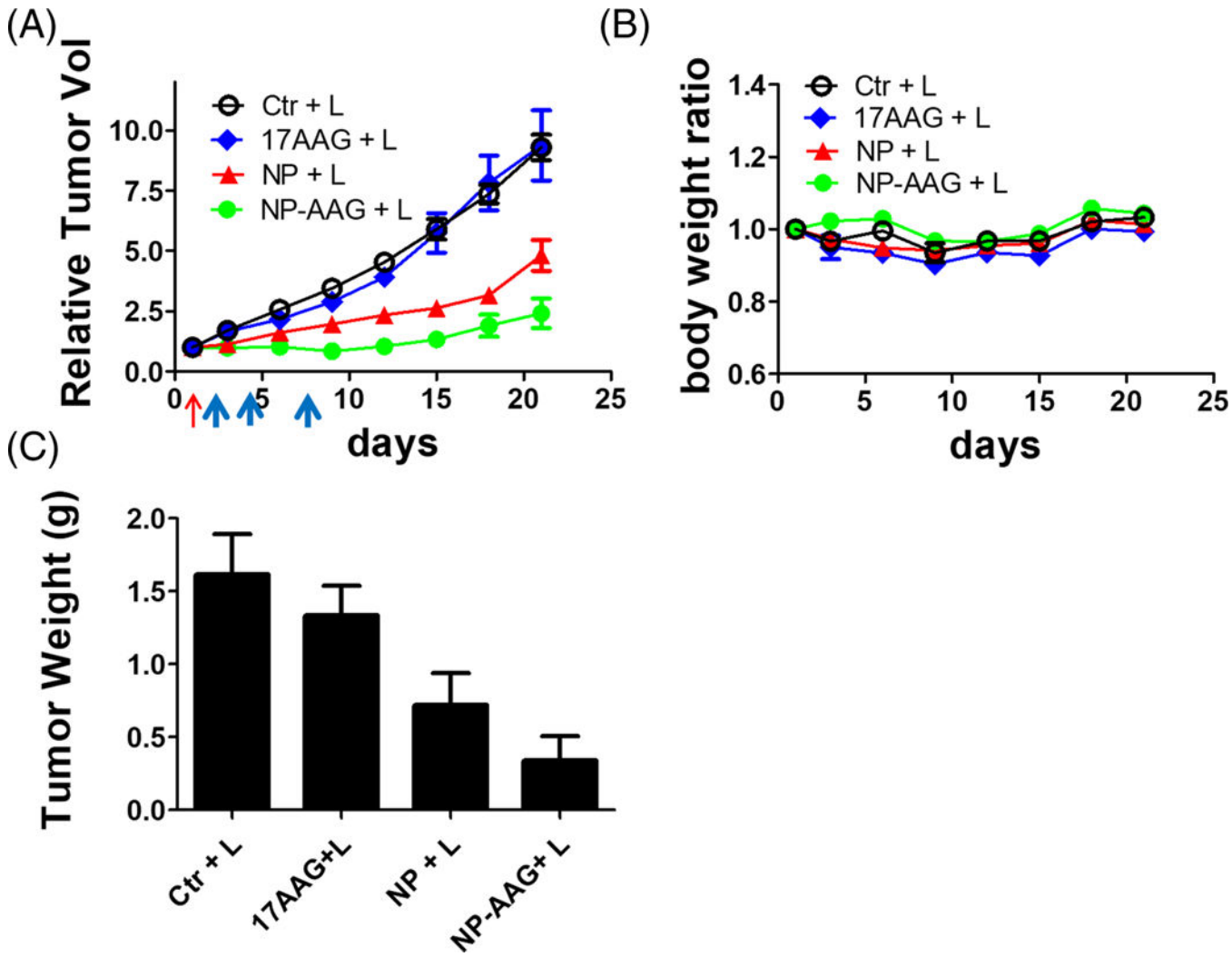

Figure 6. Anti-cancer efficacy studies of NP-AAG mediated photo-therapy in bladder cancer PDX mouse models

(A) Tumor growth curve and (B) body weight changes of mice bearing BL0382 PDX after treated with PBS, 17AAG, NP, and NP-AAG (NP: 25 mg/kg; 17AAG: 40 mg/kg) followed by the light treatment. Red arrow: Drug iv injection; Blue arrows: light treatments (680nm, 0.4W, 3 min). (C) Tumor weights harvested on day 24. Bar=1 cm (n=4)

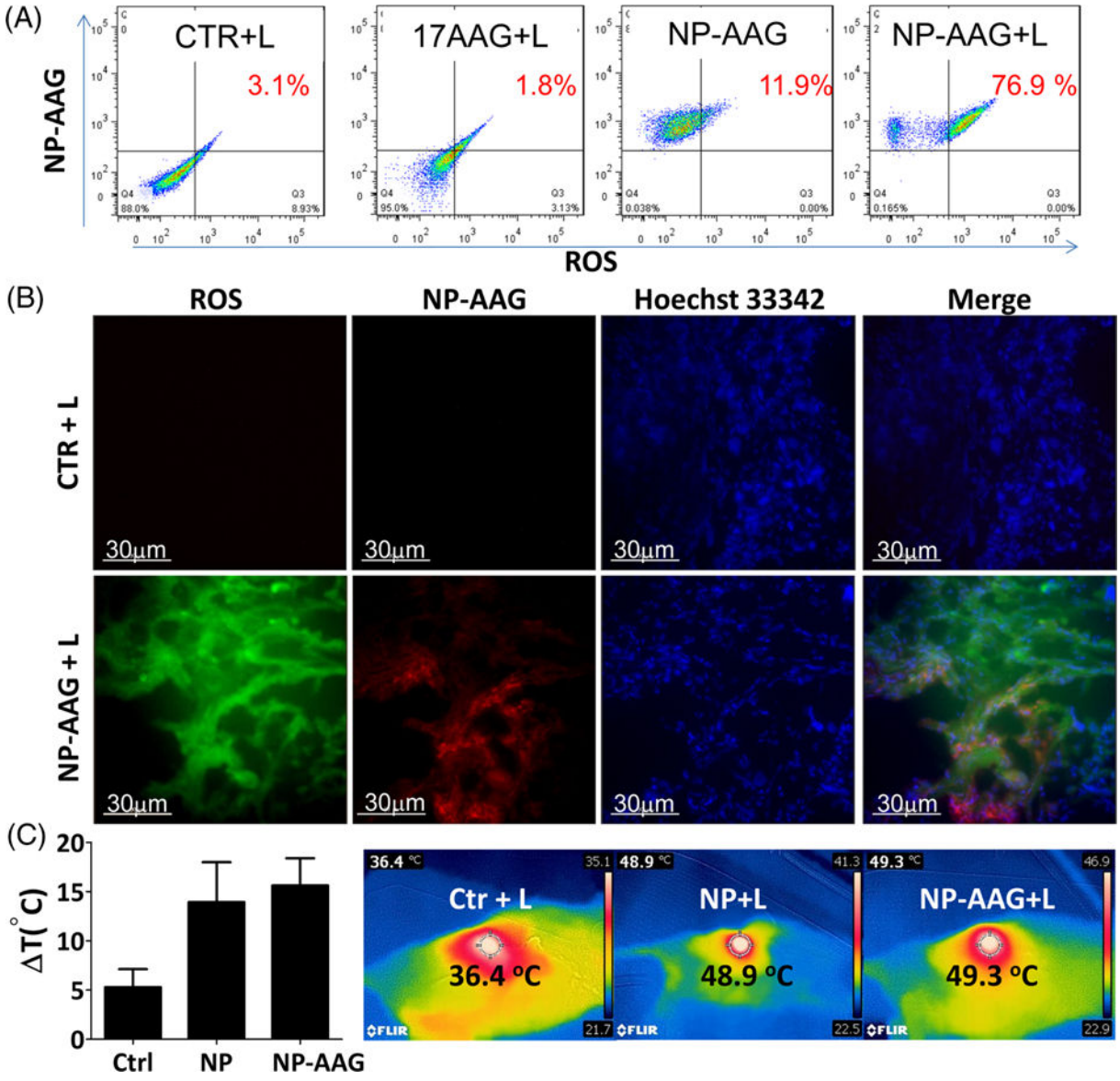

Figure 7. Mechanistic studies of NP-AAG mediated anti-bladder cancer effects

(A) Intracellular reactive oxygen species (ROS) production analysis (using ROS indicator 2′,7′-dichlorofluorescin-diacetate, DCF) upon NP-AAG mediated light treatment by flow cytometry in T24 bladder cancer cells. Cellular uptake of NP-AAG was also monitored by the increased of intrinsic NIRF signals using flow cytometry. Only cells treated with NP-AAG were NP-AAG positive. (B) ROS production in the bladder PDX cancer tissues (PBS or NP-AAG treated) upon light treatment. Mice bearing BL0382 bladder cancer were treated with PBS or NP-AAG. Tumors were harvested 48 hr later and cryosections were made. Cryosections were pre-treated with a ROS indicator (DCF) for 30 min and imaging was acquired by a DeltaVision imaging station. Hoechst 33342 was used to stain nuclei. Bar= 30 μm. (C) Tumor surface temperature changes in BL0382 bearing mice upon NP and NP-AAG mediated light treatment. Right: Representative temperature imaging. Center circle

measured the focal surface temperature and focused on the tumor area where the laser light was shed on.

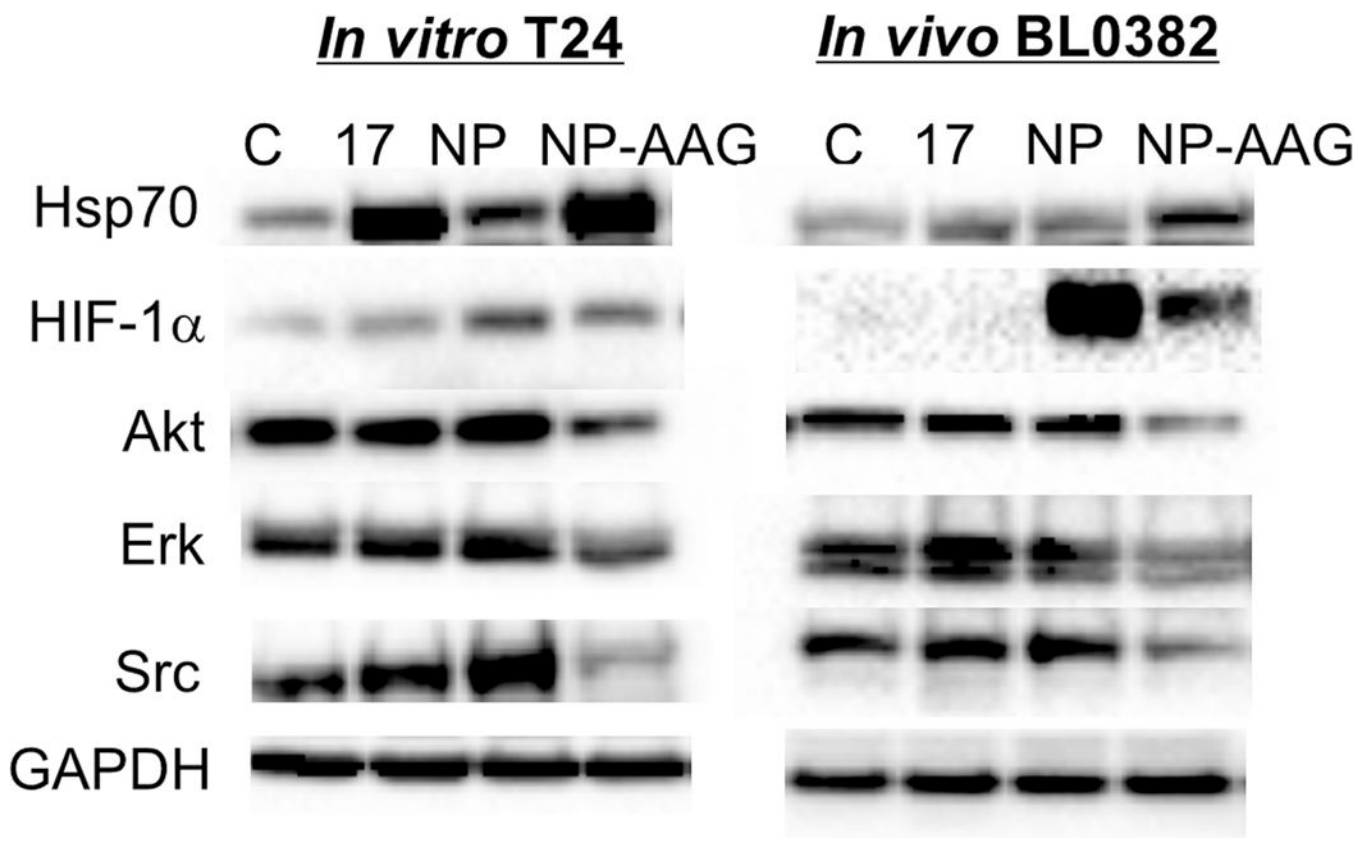

Figure 8. Molecular changes upon NP-AAG mediated photo-therapy in both *in vitro* and *in vivo*

T24 cells were treated with PBS, 17AAG, NP, NP-AAG (NP: 1 μg/mL, 17AAG: 1 μg/mL) for 8 hr followed by light treatment. Cells were collected at 12 hr post-light treatment. For the BL0382 PDX model, tumor-bearing mice were treated with PBS, 17AAG, NP, NP-AAG (NP: 25 mg/kg; 17AAG: 40 mg/kg) via tail vein. 24 hr later, tumors were illuminated with 0.4 W for 3 min. Tumors were then harvested 4 hr post-illumination. Total proteins (100 μg) were subject for western blot analysis with the antibodies indicated. GAPDH was used as the protein loading control.

Table 1

CBC profile of NSG mice treated with PBS, 17AAG, NP, and NP-AAG followed by light treatment on the third day after the last light treatment. Light: 0.4 W cm^{-2} for 3 min.

	WBC (K/ul)	RBC (M/ul)	Hematocrit %	Hemoglobin (g/dL)	Platelets (K/uL)
Ctr+L	3.7±1.12	7.1±0.54	33.7±3.23	10.2±0.79	940.8±81.65
17AAG+L	3.6±1.58	6.9±0.61	32.4±3.12	9.7±0.84	996±63.12
NP+L	3.9±0.84	7.4±0.61	34.1±3.06	10.5±0.76	921.8±47.49
NP-AAG+L	5.2±2.81	6.9±0.52	33.9±2.22	10.1±0.61	832±78.31

Table 2

Biochemistry panel of NSG mice treated with PBS, 17AAG, NP, and NP-AAG followed by light treatment on the third day after the last light treatment. Light: 0.4 W cm^{-2} for 3 min.

	Albumin g/dL	ALT (U/L)	AST (U/L)	BUN (mg/dL)	Creatinine (mg/dL)	Total Bilirubin (mg/dL)	Total Protein (g/dL)
Ctr+L	3.8±0.078	29.0±2.98	94.5±5.27	21.6±0.37	0.12±0.021	0.089±0.019	5.3±0.071
17AAG+L	3.9±0.09	23.5±4.31	68.2±13.48	21.1±1.78	0.11±0.011	0.091±0.02	5.3±0.056
NP+L	3.8±.014	26.6±6.27	80.6±32.9	22.2±0.83	0.12±0.009	0.10±0.02	5.3±0.19
NP-AAG+L	3.9±0.19	26.5±3.22	66.9±14.79	22.9±0.83	0.12±0.007	0.11±0.009	5.5±0.28